Andersen's Syndrome Mutation Effects on the Structure and Assembly of the Cytoplasmic Domains of Kir2.1[†,‡]

Scott Pegan,[§] Christine Arrabit,[||] Paul A, Slesinger,[||] and Senyon Choe*[,§]

Structural Biology Laboratory and Peptide Biology Laboratory, The Salk Institute, La Jolla, California 92037

Received April 3, 2006; Revised Manuscript Received May 17, 2006

ABSTRACT: Kir2.1 channels play a key role in maintaining the correct resting potential in eukaryotic cells. Recently, specific amino acid mutations in the Kir2.1 inwardly rectifying potassium channel have been found to cause Andersen's Syndrome in humans. Here, we have characterized individual Andersen's Syndrome mutants R218Q, G300V, E303K, and Δ314−315 and have found multiple effects on the ability of the cytoplasmic domains in Kir2.1 channels to form proper tetrameric assemblies. For the R218Q mutation, we identified a second site mutation (T309K) that restored tetrameric assembly but not function. We successfully crystallized and solved the structure (at 2.0 Å) of the N- and C-terminal cytoplasmic domains of Kir2.1-R218Q/T309K$_S$. This new structure revealed multiple conformations of the G-loop and CD loop, providing an explanation for channels that assemble but do not conduct ions. Interestingly, Glu303 forms both intra- and intersubunit salt bridges, depending on the conformation of the G-loop, suggesting that the E303K mutant stabilizes both closed and open G-loop conformations. In the Kir2.1-R218Q/T309K$_S$ structure, we discovered that the DE loop forms a hydrophobic pocket that binds 2-methyl-2,4-pentanediol, which is located near the putative $G_{\beta\gamma}$-activation site of Kir3 channels. Finally, we observed a potassium ion bound to the cytoplasmic domain for this class of K^+ channels.

Andersen's Syndrome (AS)[1] is a rare autosomal disorder in which patients exhibit electrophysiological symptoms of periodic paralysis, a prolonged QT interval, and ventricular arrhythmias (*1*, *2*). Also present in AS individuals are distinct physical abnormalities that include low-set ears, clinodactyly, scoliosis, hypertelorism, and micrognathia (*1*, *3*−*5*). AS has been directly linked to the Kir2.1 inwardly rectifying potassium channel (*4*, *5*). Point mutations occurring at one of 15 sites and two internal deletions in Kir2.1 channels have been found in patients with AS (Figure 1) (*1*−*4*, *6*, *7*). Despite their important physiological roles, the structural basis underlying molecular mechanisms of functional disorders caused by these specific mutations leading to AS have remained poorly understood.

One of the hallmarks of Kir2 channels is the strong inward rectification, in which K^+ ions flow preferentially into rather than out of the cell (*8*). Inward rectification is produced by cytosolic polyamines and Mg^{2+} occluding the ion conductance pathway as K^+ ions are flowing outward. These positively charged particles are then removed from the pore when K^+ ions flow into the cell (*9*). Rectification is the primary means of gating for Kir2 channels (*10*−*12*). The rate of rectification by these positively charged polyamine and Mg^{2+} block varies between different members of the Kir family depending on the presence of key hydrophilic residues located at two major locations. The strongest binding site of these blockers resides within the transmembrane site defined by Asp172 in Kir2.1, and weaker, recruiting sites are com-

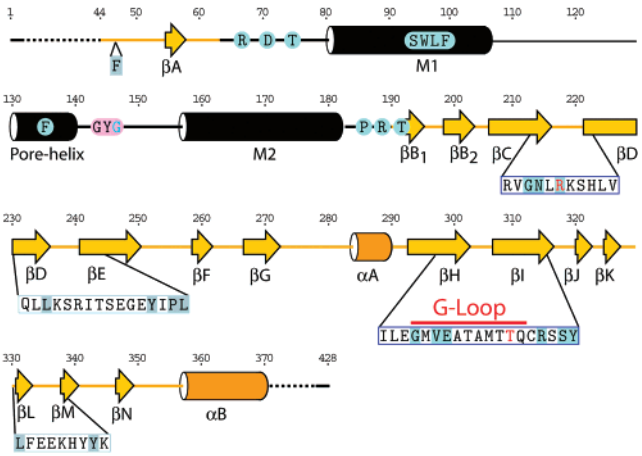

FIGURE 1: Secondary structure elements of Kir2.1 with key Andersen's Syndrome and MPD binding site locations (β-sheets in arrows and α-helices in cylinders). Those in gold are from the R218Q/T309K$_S$, added by those in black from the KirBac1.1. Shaded residues in pink denote the K^+ selectivity filter. Andersen's Syndrome sites are shaded in light blue. MPD binding sites are shaded in gray. R218Q/T309K$_S$ mutation sites are in red. Red underline represents the G-loop region.

[†] This work was supported by grants from the National Institutes of Health (P.A.S. and S.C.), National Institutes of Health Molecular Biophysics Training Grant (S.P.; GM08326), and the McKnight Endowment for Neuroscience (P.A.S.).

[‡] The coordinates of Kir2.1 (R218Q/T309K) have been deposited at the PDB (entry: 2GIX).

* To whom correspondence should be addressed. E-mail, choe@salk.edu; phone, (858) 453-4100; fax, (858) 452-3683.

[§] Structural Biology Laboratory, The Salk Institute.

[||] Peptide Biology Laboratory, The Salk Institute.

[1] Abbreviations: Kir, potassium inwardly rectifier; PIP_2, phosphylinositol 4, 5 bisphosphate; AS, Andersen's Syndrome; Kv, voltage-gated potassium (K); MPD, 2-methyl-2,4-pentanediol; Kir2.1$_L$, Kir2.1 cytoplasmic domains (44−64; 189−428); Kir2.1$_S$, Kir2.1 cytoplasmic domains (44−64; 189−371); IPTG, isopropyl-β-D-thiogalactopyranoside; DTT, dithiothreitol; wt, wild-type.

10.1021/bi060653d CCC: $33.50
Published on Web 06/22/2006

prised of several positively and negatively charged residues lining the pore in the cytoplasmic domain (*9*, *13*, *14*). The overall effect of rectification allows Kir2.1 to play a key role in eukaryotic cells by driving the resting membrane potential to E_K when the cell is at rest (*8*).

In addition to rectification, Kir channels possess other gating elements. For example, Kir2.1 channels are opened by the binding of the membrane phospholipid PIP_2 directly to the channel (*15*). Using the functional definition of gates as energetic barriers that block the permeation of potassium, we previously proposed that the flexible loop, named G-loop, at the junction between the cytoplasmic and transmembrane domains can occlude the permeation pathway as an additional gating element (*14*, *16*). Therefore, at least two energetic barriers, one located inside the pore-lining M2 helix and the other formed by the G-loop, may operate to control the ionic flow. Of the two, the G-loop is unique by being located in the cytoplasmic domains and is too narrow to permit permeation in the absence of PIP_2 (*14*). Unlike T1 domain of voltage-gated K^+ channels for which ions flow through side openings created between T1 and transmembrane domains (*17*), K ions flow through the central pore of Kir2.1 channels beginning at the cytoplasmic domain and continuing to the selectivity filter. How the G-loop and M2 helix regions work together to control ionic flow is unknown. Studies with chimeric KcsA/Kir2.1 channels indicate the cytoplasmic domain is required for Kir2.1 gating (*18*).

Biochemical data indicate that eukaryotic Kir channels form either hetero- or homotetramers (*5*, *19*). Kir2.1 channels readily form homotetramers, as well as heterotetramers with other Kir2 family members such as Kir2.2 and Kir2.3 (*5*, *20*). The ability of Kir2 subunits to assemble with AS-affected Kir2.1 subunits and restore surface expression without ion-conducting function has been a subject of recent discussion. Nonconducting heterotetramers containing AS-affected Kir2.1 subunits indicate that the AS-affected Kir2.1 subunits provide a dominant-negative effect on the channels (*5*). Furthermore, a recent report showed that AS-affected Kir2.1 channels-carrying mutants, D71V, Δ95−98, S136F, G144S, N216H, R218Q, G300V, V302M, E303K, and Δ314−315, were largely incapable of reaching the membrane by themselves; but G144S, N216H, G300V, and E303K could be transported successfully if coexpressed with wild-type (wt) Kir2.1 (*21*). Nevertheless, these channels were all nonconducting like the heterotetrameric Kir2.x channels containing AS-affected Kir2.1 subunits (*5*, *21*) (but see ref *2*). The loss of functional Kir2 channels on the membrane can clearly alter membrane excitability in many tissues, such as in heart (*22*).

The mechanism by which wt Kir2.1 and Kir2.3 channels recover surface expression with some AS-affected Kir2.1 channel subunits but impair channel activity is not well-understood. On the basis of the structure of the N-terminal and C-terminal domains of wt Kir2.1 at 2.4 Å, (*14*) we previously proposed that AS mutations could interfere with the function of the G-loop and thereby alter gating. On the basis of electrophysiological studies of full-length channels, the flexibility of the pore-facing G-loop appeared to be essential for proper channel function. (*14*). Alternatively, we suggested that some of these AS mutations such as R218Q may interfere with the ability of the channel to form a tetramer. In the present study, we have used biochemical techniques to probe how four cytoplasmic AS mutations in Kir2.1, R218Q, G300V, E303K, and Δ314−315, impact the stability of functional tetrameric channels. For one mutation, R218Q, we have determined that a second site mutation, T309K, can rescue tetrameric assembly but does produce functional channels. We describe the atomic structure of the Kir2.1 cytoplasmic domain containing two mutations, R218Q and T309K, which provides additional evidence implicating the G-loop in gating and tetrameric assembly. In the course of this study, we found a novel ligand bound to a biologically relevant site in the C-terminal domain. Finally, the 2.0 Å structure also places a single potassium ion in the cytoplasmic domain of the ion-permeation pathway, which may affect K^+ permeation.

EXPERIMENTAL PROCEDURES

Molecular Biology and Protein Purification. Fusion constructs $Kir2.1_S$, N-terminal (44−64) and C-terminal (189−371), and $Kir2.1_L$, N-terminal (44−64) and C-terminal (189−428), were generated from mouse Kir2.1 (Figure 1) and linked through two-step PCR prior to being cloned into an octa-histidine expression vector modified from pet28a (Invitrogen). Andersen's Syndrome mutations were incorporated via Quick-Change Site-directed Mutagenesis Kit (Stratagene).

Kir2.1 mutants were grown in Terrific Broth at 37 °C to the OD_{600} of 0.6, then induced with 0.5 mM IPTG for 3 h prior to harvesting. Cells were lysed in 0.5 M NaCl, 20 mM Tris-HCl, pH 8.5, 10% glycerol, 7 mM β-mercaptoethanol, 0.1 mM PMSF, 10 mM imidazole, and 0.5 mg lysozyme per 100 mL of lysate. The lysate was sonicated and spun at 94 000*G* for 45 min. The supernatant was loaded on a 2 mL-packed nickel affinity column (Qiagen), washed with 5 mL of lysis buffer without PMSF, and then eluted with lysis buffer with 250 mM imidazole. Thrombin was added to the eluted fraction and it was dialyzed against the sizing column buffer, 150 mM NaCl, 5 mM Tris-HCl, pH 8.5, 2 mM DTT. Kir2.1 was then purified by S200 Sepharose chromatography and concentrated to 10 mg/mL with 10 mM DTT. Kir2.1 proteins were loaded onto a G4000PWXL HPLC column (TOSOH) equilibrated in 150 mM NaCl, 5 mM Tris-HCl, 8.5, and 2 mM DTT. Molecular weight (MW) of the tetramer complex was calculated by Minidawn static light scattering requiring the use of the extinction coefficient of the monomer. The extinction coefficient was derived from the primary sequence of the protein.

Crystallography. $Kir2.1_S$-R218Q/T309K (R218Q/$T309K_S$) was crystallized in the space group *C*2 at 4 °C by vapor diffusion with hanging drops mixed 1:1 with 35% 2-methyl-2,4,pentanediol (MPD), 0.1 M Na/KPO_4, pH 6.2, and 50 mM NaCl. Crystals were placed in a precipitation solution for 15 s prior to flash-freezing in liquid nitrogen. Data sets were collected for R218Q/$T309K_S$ and R218Q/$T309K_L$ at Advanced Light Source (ALS), Berkeley, CA, and Stanford Linear Accelerator Center (SSRL), respectively. Molecular replacement solutions were derived using the model of wt $Kir2.1_L$ by Phaser. The final model was refined with the 2.0 Å data from R218Q/$T309K_S$ by the software CCP4 suite.

Electrophysiology. Full-length wt Kir2.1 and the following point mutants, R218Q, T309K, T309R, R218Q/T309R, and R218Q/T309K, were constructed in pBSK using PCR (*23*).

All constructs were confirmed by DNA sequencing. In vitro methyl-capped cRNAs were synthesized from linearized cDNA and transcribed with T3 RNA polymerase (Stratagene). The quality of cRNA was estimated using an ethidium-stained formaldehyde gel. Oocytes were isolated from *Xenopus laevis* frogs as described previously (*24*). The experimental procedure was approved by the IACUC at The Salk Institute. Oocytes were injected with a 46 nL solution containing cRNA for the Kir2.1 channels (0.5−5 ng) and incubated in ND96 (96 mM NaCl, 2 mM KCl, 1 mM $CaCl_2$, 1 mM $MgCl_2$, and 5 mM HEPES, pH 7.6, with NaOH) for 1−4 days at 16 °C.

Macroscopic currents were recorded using the two-electrode voltage-clamp method as described previously (*24*). Briefly, currents were recorded from oocytes with Geneclamp 500 amplifier (Axon Instruments), filtered at 0.05−2 kHz, digitized (0.1−2 kHz) with a Digidata 1200 A/D interface (Axon Instruments), and stored on a laboratory computer. Electrodes were filled with 3 M KCl and had resistances of 0.6−1 MΩ. Oocytes were perfused continuously with an extracellular "95K" solution (90 mM KCl, 2 mM $MgCl_2$, and 10 mM HEPES, pH 7.5, with ∼5 mM KOH), "2K" solution (2 mM KCl, 88 mM NaCl, 2 mM $MgCl_2$, and 10 mM HEPES, pH 7.5, with ∼5 mM NaOH), or "95Na" solution (90 mM NaCl, 2 mM $MgCl_2$, and 10 mM HEPES, pH 7.5, with ∼5 mM NaOH). The 95Na was used to determine the leakage current and subtracted directly from the currents measured in 95K and 2K. A small chamber (0.125 × 0.600 in.) with fast perfusion was used to exchange the extracellular solution and was connected to ground via a 3 M KCl agarose bridge. Macroscopic currents were elicited with 150 ms voltage-steps from −100 mV to +50 mV. Mutants were studied in 2−3 different batches of oocytes. The current amplitude was measured at the end of a 150 ms step pulse. All values are given as mean ± SEM.

RESULTS

Effects of AS Mutations on the Assembly of the Cytoplasmic Domains of Kir2.1. To investigate the effect of specific AS mutation on the tetrameric assembly of the channel, AS mutations R218Q, G300V, E303K, and Δ314−315 were introduced individually into the $Kir2.1_L$ construct (N-terminal 44−64 fused to C-terminal 189−428; Figure 1). Of these mutants, R218Q, G300V, and E303K were selected on their ability to traffic to the cell membrane when coexpressed with wt Kir2.1 and their proposed roles in gating (G300V), forming intra- (R218Q) and intersubunit (E303K) interactions (*14*, *21*). The Δ314−315 was chosen because it does not allow proper trafficking when coexpressed with wt. Each of these mutations has a distinct effect on the quaternary state of the channel's cytoplasmic domains. Δ314−315 in $Kir2.1_L$ ($\Delta 314-315_L$) resulted mostly in misfolded protein. R218Q ($R218Q_L$) produced mildly larger aggregates (Figure 2b). Unlike $\Delta 314-315_L$ and $R218Q_L$, $E303K_L$ produced significant amounts of soluble tetrameric protein. Interestingly, $E303K_L$ eluted earlier than wt on S200 Sepharose size chromatography (designated as profile 2 in Figure 2b). The $G300V_L$ also eluted to the left of the wt reproducibly, but not to the same extent as the E303K, and was designated as profile 1. G300V and E303K without the flexible tail (truncated at position 372 named as $Kir2.1_S$ (*14*)), showed a similar left shift in their elution, indicating that these changes

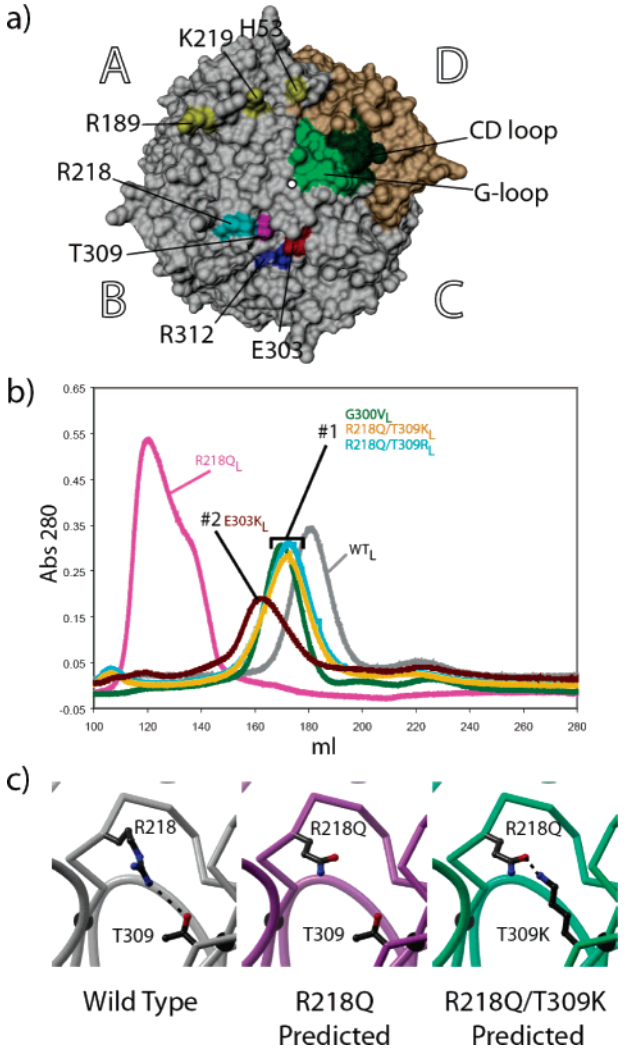

FIGURE 2: Sizing chromatograms of various mutants of $Kir2.1_L$ by S200 Sepharose column (void volume at 105 mL). (a) Top down view of a cytoplasmic domain surface rendering of the structure of wt $Kir2.1_L$. Monomer D is highlighted in light brown. The G-loop and CD loop of Monomer D are colored in green and dark green, respectively. PIP_2-binding in monomer A is highlighted in yellow. The Thr309, Arg218, and Arg 312 are colored in monomer B magenta, cyan, and blue, respectively. Glu303 is colored red in monomer C. The ∼2.9 Å opening of the G-loop is represented by a black circle. (b) wt $Kir2.1_L$ (gray), $E303K_L$ (red), $R218Q_L$ (magenta), $G300V_L$ (green), $R218Q/T309R_L$ (teal), and $R218Q/T309K_L$ (gold). (c) Close-up of positions Arg218 and Thr309 in the wt $Kir2.1_L$ structure (gray), predicted models of $R218Q_L$ (violet), and $R218Q/T309K_L$ (teal). Dashed lines represent polar interactions.

were not caused by the flexible C-terminal tail of $Kir2.1_L$ (residues 373−428). Attempts to crystallize G300V and E303K were unsuccessful. However, these results already demonstrate the two Kir2.1 AS mutations cause the cytoplasmic domain to adopt conformations that are distinct from that of the wt species.

To understand the nature of the mildly aggregating R218Q, we reasoned that changing the Thr309 to a positive charge residue would restore a polar interaction similar to the native one present in Kir2.1 between Arg218 and Thr309 (Figure 2c). Here, we examined the electrophysiological properties of these mutants. Two-electrode voltage clamp was used to record macroscopic currents in oocytes injected with cRNA for Kir2.1 or Kir2.1 mutants. We previously showed that additional change to Lys or Arg at Thr309 could restore the

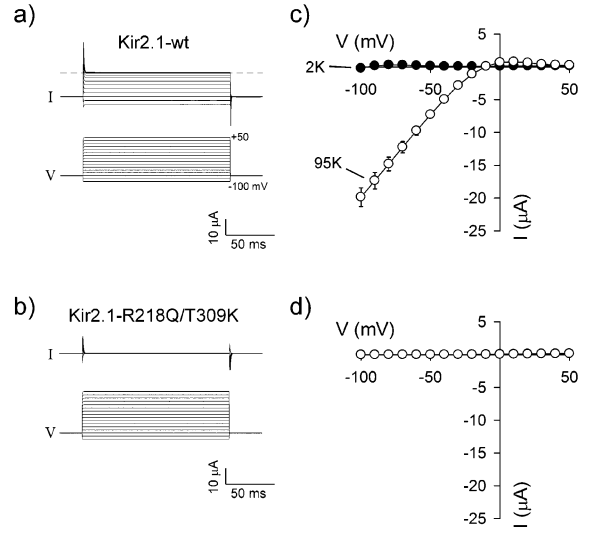

FIGURE 3: Inwardly rectifying K^+ currents detected for Kir2.1-wt but not for Kir2.1-R218Q/T309K channels expressed in *Xenopus* oocytes. Two-electrode voltage-clamp was used to record macroscopic currents from oocytes injected with cRNA for Kir2.1-wt, Kir2.1-R218Q, Kir2.1-T309K, or Kir2.1-R218Q/T309K. (a and b) Representative examples of current (I) and voltage (V) traces are shown for the Kir2.1-wt (a) and Kir2.1-R218Q/T309K mutant (b) channels. Macroscopic currents were elicited by voltage steps from −100 mV to +50 mV in the 95 K extracellular solution. The holding potential was −80 mV. Dashed line indicates zero current level. (c and d) The average currents are plotted as a function of voltage for Kir2.1-wt (c, $n = 10$) and Kir2.1-R218Q/T309K mutant (d, $n = 10$) channels. Average currents at −100 mV were -0.21 ± 0.01 μA in 2 K and -19.87 ± 1.43 μA in 95 K for wt ($n = 5$), -0.011 ± 0.002 μA in 2K and -0.036 ± 0.002 μA in 95K for R218Q ($n = 10$), -0.009 ± 0.002 μA in 2 K and -0.036 ± 0.003 μA in 95 K for T309K ($n = 10$), and -0.011 ± 0.003 μA in 2 K and -0.039 ± 0.020 μA in 95 K for R218Q/T309K ($n = 10$).

tetrameric assembly of the $Kir2.1_L$ (*14*). Interestingly, however, both R218Q/T309R and R218Q/T309K did not restore the wt current of the channel (Figure 3). Furthermore, it was apparent from the sizing column that the extent of conformational change in $Kir2.1_L$-R218Q/T309K (R218Q/$T309K_L$) or $Kir2.1_L$-R218Q/T309R (R218Q/$T309R_L$) is similar to $G300V_L$, profile 1, as they both eluted nearly at the same position. These results lead to the idea that these two double mutants share an altered nonfunctional conformation, as with G300V, that disrupts channel function.

G-Loop Conformation of a Double Mutant R218Q/T309K. The ability of the R218Q/T309K and R218Q/T309R to restore the native tetrameric state of the cytoplasmic domains, but be trapped in an altered conformation (profile 1; Figure 2b) and fail to rescue channel function, suggests that Arg218 may play a more complex role than just forming a stable tetramer. Furthermore, the $G300V_L$-like profile and proximity of Arg218 to the G-loop structure suggested that mutation of R218Q may be affecting the flexible G-loops in the same way as the G300V mutation. To resolve the molecular impact of the R218Q mutation, we sought to obtain X-ray crystal structure of the isolated, R218Q/$T309K_L$ and R218Q/$T309R_L$. Both R218Q/$T309K_L$ and R218Q/$T309R_L$ produced crystals in 35% *tert*-butyl alcohol (0.1 M citrate, pH 5.2, 0.2 M $MgCl_2$), in the I4 space group, which diffracted to 6.0 Å in one direction and 4.0 Å in the other. Subsequently, crystals of the R218Q/$T309K_S$ lacking the 56 C-terminal residues of $Kir2.1_L$ grew in a 35% MPD, 50 mM NaCl, 0.1 M Na/KPO_4 condition in the *C*2 space group, diffracting to 2.0 Å resolution ($a = 140.67$ Å, $b = 98.82$ Å, $c = 98.09$ Å; $\alpha = 90°$, $\beta = 130.68°$, $\gamma = 90°$). We have determined the structure of R218Q/$T309K_S$. There is one tetramer per asymmetric unit containing 818 residues, 713 waters, four MPD molecules, and one K^+ ion (Table 1).

Table 1. Crystallographic Data for R218Q/$T309K_S$

data collection	
protein/data set	R218Q/$T309K_S$
space group	*C*2
cell constants	$a = 140.67$ $b = 98.87$ $c = 98.09$ $\alpha = \gamma = 90$ $\beta = 130.68$
wavelength (Å)	1.000
source	ALS
resolution (Å)	2.0
total observations/total reflections	238256/66107
completeness (highest-resolution shell)	99.45 (94.17)
I/σ (highest-resolution shell)	13.4 (2.7)
R_{sym}[a]	0.086
model refinement	
total reflections (reflections for test)	62743 (3363)
R_{work} (%)/R_{free} (%)[b]	17.8/23.0
protein atoms/water atoms	6546/ 713
rms deviation of bond lengths (Å)	0.018
rms deviation of bond angles (°)	1.65

[a] $R_{sym} = \sum_h \sum_i |I_i(h) - \langle I(h)\rangle| / \sum_h \sum_i I_i(h)$, where $I_i(h)$ is the ith measurement and $\langle I(h)\rangle$ is weighted mean of all measurements of $I(h)$. [b] $R_{free} = h(|F(h)_{obs}| - |F(h)_{calc}|)/h|F(h)_{obs}|$ for reflections in the working and test sets, respectively. rms, root-mean-square.

The overall scaffold of R218Q/$T309K_S$ is similar to that of the wt $Kir2.1_L$ (Figure 4a,b). Closer inspection of the two structures show five regions that differ significantly (Figure 4c,d). One of these regions was the linker between N- and C-terminal domains; the electron density supported only the main chain placement with high-temperature factors, suggesting higher flexibility of the region. Two other regions included the loop between β-sheet D and β-sheet E (DE loop) and the region from the beginning of the β-sheet L to β-sheet M (LM loop) (Figure 4c; see below). The two most intriguing sections are located at the G-loop and CD loop (Figure 4c).

Intriguingly, these structural changes are nonuniform in each subunit. G-loops of monomers B and D collapsed toward the center of the pore reducing the pore size of channel from 5.7 to 3.6 Å between the carboxyl oxygen of Ala 304 of monomer B and C_β of Ala 304 in the monomer D (Figure 4d). In contrast to the monomers B and D collapsing in, the monomers A and C are displaced away from the center of the channel to a more open conformation resulting in a 9.41 Å distance between their C_β of Ala 304. G-loops of all four subunits have relatively lower temperature factors than those in the wt structure. Closer inspection of the G-loop and CD loop regions shows that β-sheet I backbone containing T309K is unperturbed, and the conformational change is restricted to the CD loop containing R218Q and the G-loop (Figure 5a,b). Monomer D subunit regains the polar interaction between R218Q and T309K as predicted in Figure 2c (Figure 5b). Surprisingly, the other three monomers have a mix of conformations, with monomers A and B having relatively higher temperature factors

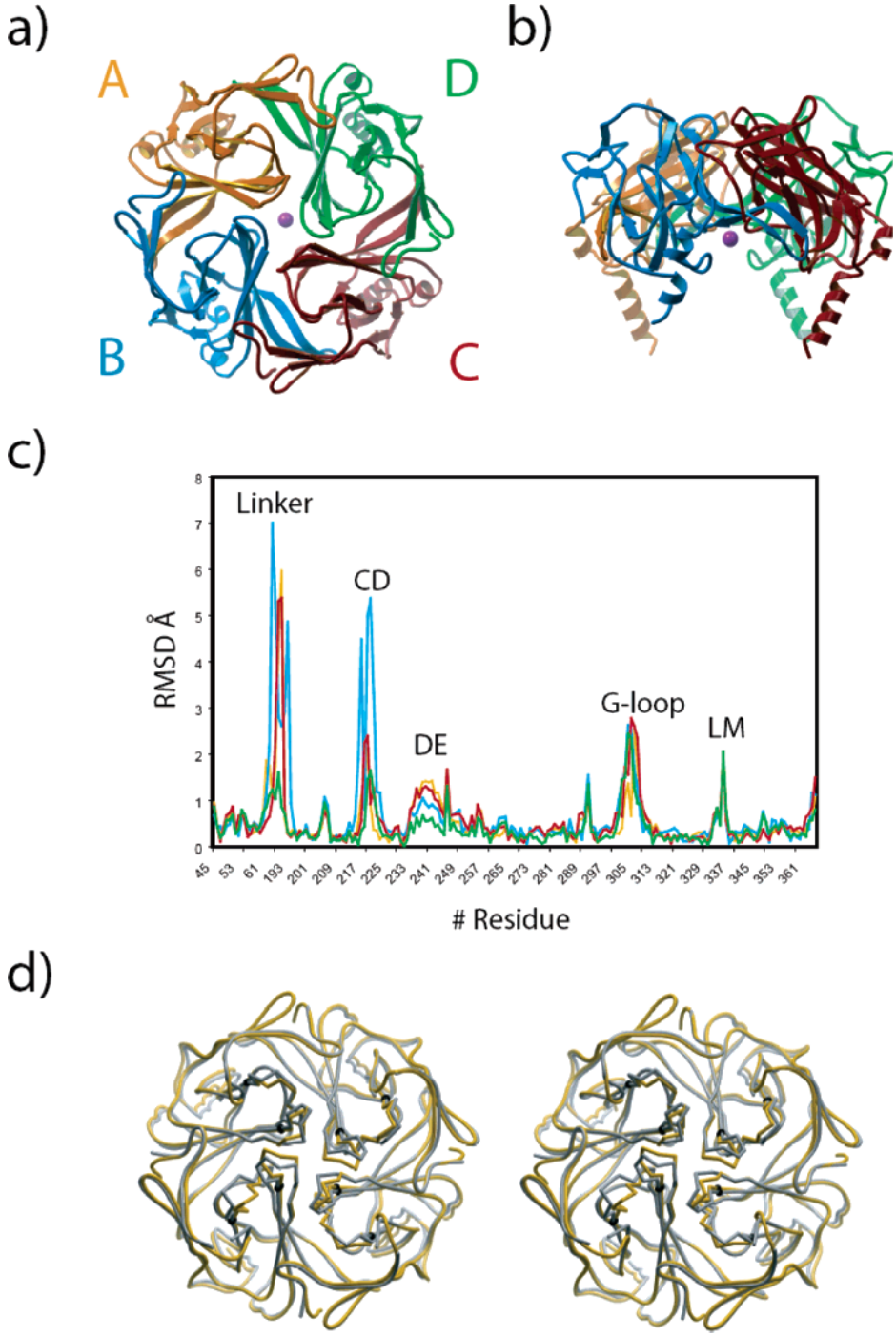

FIGURE 4: R218Q/T309K$_S$ structure. (a) Top view of R218Q/T309K$_S$ tetramer; monomers A (gold), B (blue), C (red), D (green); K^+ ion is represented in purple. (b) Side view of R218Q/T309K$_S$ tetramer. K^+ ion is represented in purple. (c) Root-mean-square deviations between Kir2.1$_L$ to R218Q/T309K$_S$ monomers A (gold), B (blue), C (red), D (green). (d) Stereoview of Kir2.1$_L$ (gray) and R218Q/T309K$_S$ (gold) to highlight the G-loop conformation variations near the pore.

than the wt. These nonuniform conformational changes of the CD loop and the reduced temperature factors of the displaced G-loops observed in the R218Q/T309K$_S$ structure result in asymmetrical displacement of the G-loop with a smaller opening than that of the wt Kir2.1$_L$ channel.

Disruption of K219 by R218Q Creates Different Salt Bridge Partners for E303K. In the wt structure, Lys219 side chain points into a void that is expected to be a putative PIP_2 binding site and Arg218 points also out of the site (*2*, *14*). In the R218Q/T309K$_S$ structure, Lys219 in monomers A, B, and D are highly flexible (Figure 5a,b). In contrast, the Lys219 in the monomer C has a low-temperature factor (electron density peak at 1.7 σ) and interacts with the carboxyl oxygen of intrasubunit Val56, rotated 180° from its wt orientation. Like Lys219, Glu303 also shows a nonuniform difference in position. As a result, we observe two different conformations of the G-loop near the Glu303. In the wt, as with monomers A and B of R218Q/T309K$_S$, Glu303 forms a salt bridge to Arg 312 across monomer to monomer. The other conformation shows that E303K of monomer C interacts with His221 of the C subunit forming the intrasubunit charge pair (Figure 5c). These local disparities contribute to the formation of the asymmetric disposition of the G-loops (Figure 4d).

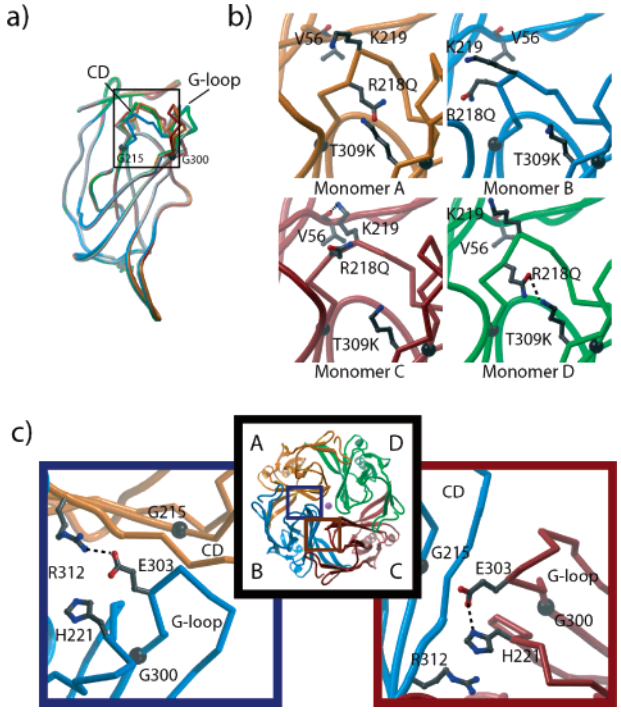

FIGURE 5: Close-up near Arg218 and Thr309. (a) R218Q/T309K$_S$ monomers A (gold), B (blue), C (red), and D (green). (b) Close-up views of the boxed area in (a) near Arg218 and Thr309 positions. Dashed lines represent polar interactions. (c) Close-up view near Glu303 between monomers, A and B (left), or B and C (right). Dashed lines represent salt bridges.

2-Methyl-2,4-pentanediol (MPD). As stated earlier, the DE and LM loops are two of the regions that are divergent between the wt Kir2.1$_L$ and R218Q/T309$_L$ structures (Figure 4c,d). Both regions form key interactions between adjacent monomers. Examination of the DE and LM loops identified electron density attributed to MPD. The distinct *C*2 tetrahedral coordination of MPD coupled with the resulting stereochemistry of the C4 atom allows easy placement within the density with agreeable ($F_o - F_c$) density (Figure 6b). Extensive interactions of MPD with the solvent-accessible site show H-bonding and hydrophobic interactions pull the DE and LM loops closer together (Figure 6b). O2 atom of MPD contacts Tyr337. The other oxygen atom O4 of MPD forms H-bond interactions with the carbonyl oxygen of Pro244 and Tyr242 via water. Phe47, Leu232, Leu245, and Leu330 provide the hydrophobic interactions with the methyl groups of MPD.

K^+ Binding at the Cytoplasmic Pore Entrance. Analysis of the electron density present in the pore of R218Q/T309K$_S$ revealed a single K^+ at the cytoplasmic end of the pore (Figure 4b). Surprisingly, the coordination of the K^+ is not formed by anionic residues in the pore, but is mediated through eight caging waters. These waters are arranged in an antiprism arrangement, with four located on the cytoplasmic side of the potassium ion and the other four located internally to the pore, similar to that of backbone- and water-coordinated K^+ of previous KcsA transmembrane structures (Figure 6c, d) (*25*). The electron density in $F_o - F_c$ maps is consistent with K^+ present during purification and crystallization. Placement of Na^+, the only other cation in the crystallization buffer, and biologically relevant Mg^{2+} in the position of K^+ would not account for electron density in the

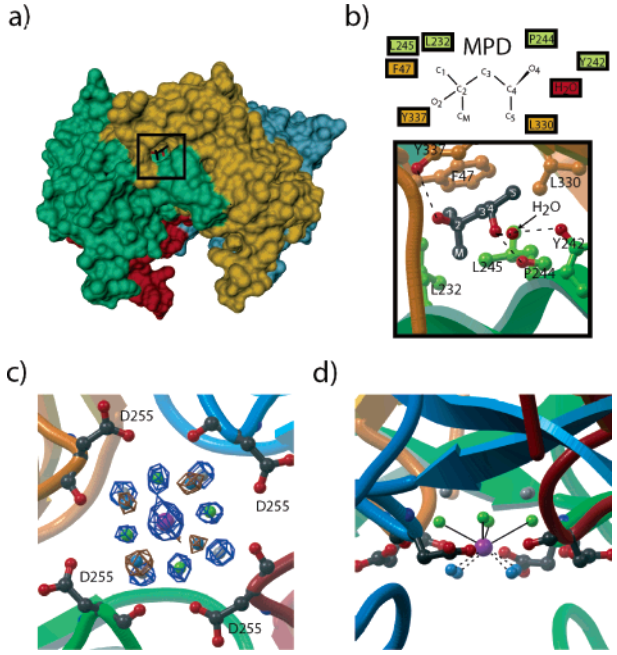

FIGURE 6: MPD and water-caged K^+ binding sites. (a) Standard side view of R218Q/T309K$_S$ as in Figure 4b. (b) MPD binding site residues in box of (a). Dashed lines represent polar interactions. (c) Bottom-up view of K^+ binding site with experimental electron density showing 12 waters, K^+, and Asp255 in ball-and-stick. Blue electron density maps are at 2.9 σ and brown at 1.7 σ for clarity. K^+ is rendered in purple. Waters are colored with respect to the layer they comprise. The cytoplasmic waters (light blue) are 412, 498, 266, and 427. The first-layer waters inside the pore (green) are 89, 75, 80, and 121. The second-layer pore waters (gray) are 85, 76, 58, and 47. (d) Side view of (c). Dashed lines represent cytoplasmic water bonds that range from 2.65 to 2.87 Å. Solid lines represent pore water bonds that range from 2.77 to 3.03 Å. These eight waters form antiprism geometry that coordinates the potassium ion.

$F_o - F_c$ maps, nor the 2.69−2.89 Å optimum bond distance to the water molecules typical of K^+ coordination (*26*). All of these waters are coordinated via H-bonds to the anionic side chain and backbone carboxyl oxygen of Asp255. The presence of the water-caged K^+ completely occluding the pore establishes this site as the first binding site in the K^+ permeation pathway toward the selectivity filter.

DISCUSSION

In the current study, we have used biochemical and electrophysiological techniques to examine R218Q, G300V, E303K, and Δ314−315 AS mutants and have found multiple effects on the ability of the cytoplasmic domains in Kir2.1 channels to form proper tetrameric assemblies, which we propose involves displacement of the G-loop. In addition, we have discovered a novel ligand binding site in Kir2.1 as well as located the first K^+ ion in the cytoplasmic pore structure.

Significance of Asymmetry in AS Mutants. For the R218Q AS mutant, we hypothesized that changing the Thr309 to a positively charged residue (Lys) would restore a polar interaction found in wt Kir2.1 between Arg218 and Thr309 (Figure 2c). Sizing chromatography and structural (2.0 Å) analyses of R218Q/T309K$_S$ revealed the presence of a significant asymmetrical conformation at a critical region (G-loop) in the permeation pathway. Both this and the previous structure (*14*) were solved as tetramers in the asymmetric

unit, allowing the subunit to be refined independently of each other. In two of the four subunits, the G-loop is displaced from its normal position. This arrangement may explain why the tetrameric assembly of the Kir2.1 channel's cytoplasmic domains is insufficient to restore ion-conducting functionality. The G-loop is anchored at one end by a flexible Gly at position 300, which we speculate allows the G-loop to pivot (*14*). The other end of the G-loop lacks a single flexible amino acid. Here, the inter-loop side chain interactions are formed by two sets of binding pairs, Arg218/Thr309 and Glu303/Arg312, which form both intersubunit salt bridges between G-loops and intrasubunit polar interactions with the CD loop. This suggests that mutations that alter these interactions would result in a displaced G-loop and a nonfunctional pore. Consistent with this, a T309I mutation was recently identified in patients with AS (*27*).

Arg218 has also been implicated in binding PIP_2 and gating of Kir2.1 (*2*). Altering the interaction between Arg218 and Thr309 could alter the ability of Arg218 to stabilize PIP_2 binding. On the basis of the observations that Glu303 can form different salt bridges, with Arg312 or His221, and that Arg218 interacts with Thr309, we speculate that the binding of PIP_2 to Lys219 induces the movement of the CD loop, which alters the position of the G-loop through the Arg218/Thr309 interaction. The Glu303 residue would then break its intersubunit salt bridge to create a new intrasubunit one with His221, compensating for the energetic cost of breaking the previous salt bridge and allowing the G-loop greater flexibility. These actions would allow the G-loop aperture to open enough for hydrated K^+ ion to pass. These studies provide a plausible mechanism for PIP_2 gating; however, future experiments are needed to work out the details of PIP_2-dependent gating of Kir2.1 channels.

In order for Kir channels to influence membrane excitability, they must be first targeted properly to the plasma membrane. Interestingly, specific AS-affected $Kir2.1_L$ cytoplasmic domain mutants that can form tetramers appear to be trafficked properly to the membrane in their full-length form (*5*, *21*). The inability of Δ314−315 AS-affected Kir2.1 channels to reach the membrane (*21*) and our finding that $\Delta 314{-}315_L$ is mainly expressed in the inclusion bodies are consistent with the interpretation that Δ314−315 Kir2.1 channels are misfolded and cannot form a tetramer in the absence or presence of wt subunits, prior to leaving the endoplasmic reticulum. On the other hand, both G300V and E303K, which can form stable homotetramers with their cytoplasmic domains, have been shown to be successfully trafficked to the membrane (*2*, *5*, *21*). When coexpressed with wt channel subunits, the heteromers either do not function or have impaired function (*5*, *21*) (but see ref *2*). The $R218Q/T309K_S$ structure suggests that the ability to attain the symmetry of Kir2.1 cytoplasmic domains near the G-loop gate is required for the proper function of the channel. This would explain how heteromeric channels carrying AS-affected subunits can be trafficked properly to the cell surface but remain nonconducting (*5*, *21*).

Novel MPD Binding Pocket in Kir2.1—R218Q/T309K$_S$ Structure. During the course of our AS mutant study, we discovered a small molecule of MPD bound to the cytoplasmic domain. MPD was found in all four subunits of $R218Q/T309K_S$, in a hydrophobic pocket formed by amino acids in the DE and LM loops. A comparison between $R218Q/T309K_S$ and the wt $Kir2.1_L$ structures suggests that MPD induces a structural change in the Kir2.1 channel that brings the DE and LM loops closer toward each other (Figure 4c). If MPD induces structural changes in Kir2.1 cytoplasmic domains, then MPD could affect the gating properties of the full-length channel. The hydrophobic residues interacting directly with MPD are conserved between the Kir2 and Kir3 families. Two amino acids, Pro244 and Tyr337, form H-bonds with the hydroxyl groups of MPD and are conserved in Kir2.1 and Kir3.2 but differ in Kir3.1 (Figure 1). Interestingly, these loops have been previously shown to be part of a putative $G_{\beta\gamma}$ activation site in Kir3 channels (*24*). Whether the binding of MPD or analogues to this site will activate or suppress Kir channels is unknown. With the likely presence of the MPD site in both Kir2 and Kir3 channels and its location near the putative $G_{\beta\gamma}$ G-protein activation site, MPD could be exploited as a framework to design a novel drug to modulate Kir2 and/or Kir3 channels.

Hydrated K$^+$ Bound to Asp255 in Kir2.1—R218Q/T309K Structure. Previous X-ray structural studies of KirBac1.1 have uncovered K^+ ions in the selectivity filter (*16*). K^+ ions were not resolved in the cytoplasmic domains of KirBac1.1, Kir3.1, or Kir2.1 (*14*, *16*, *28*). Most likely, the lack of K^+ ions in the crystallization buffer of Kir3.1 and Kir2.1 can explain the absence of this ion in the structure (*14*, *16*, *28*). For KirBac1.1, two residues are absent in the loop that form the cytoplasmic end of the pore, resulting in a wider opening that may not coordinate a hydrated K^+ ion through the waters of the first hydration shell (*16*). Finding a single hydrated K^+ ion in the inner vestibule of Kir2.1 along the permeation pathway is intriguing because of the known conduction properties of K^+ channels. Potassium ions and polyamines are focused on the central water-filled canal leading to the selectivity filter. The central location and exact coordination of the K^+ suggest the ion permeation pathway of the cytoplasmic domain is more like a set of stops mediated by both waters and anionic side chains, not a hydrophilic wall that only recruits K^+ ions at random sites along its wall (*9*, *12*, *13*). Asp255 represents one of the first positions along this permeation pathway for both polyamines and potassium ions. Although the 'long-pore' effect of K^+ channels is attributed to the multiple potassium ions located in the selectivity filter, the presence of the hydrated potassium ion along the central canal demonstrates that the long pore indeed extends quite far into the cytoplasm.

REFERENCES

1. Plaster, N. M., et al. (2001) Mutations in Kir2.1 cause the developmental and episodic electrical phenotypes of Andersen's syndrome, *Cell 105* (4), 511−519.
2. Lopes, C. M., et al. (2002) Alterations in conserved Kir channel-PIP2 interactions underlie channelopathies, *Neuron 34* (6), 933−944.
3. Donaldson, M. R., et al. (2003) PIP2 binding residues of Kir2.1 are common targets of mutations causing Andersen syndrome, *Neurology 60* (11), 1811−1816.
4. Tristani-Firouzi, M., et al. (2002) Functional and clinical characterization of KCNJ2 mutations associated with LQT7 (Andersen syndrome), *J. Clin. Invest. 110* (3), 381−388.
5. Preisig-Muller, R. et al. (2002) Heteromerization of Kir2.x potassium channels contributes to the phenotype of Andersen's syndrome, *Proc. Natl. Acad. Sci. U.S.A. 99* (11), 7774−7779.
6. Hosaka, Y. (2003) Function, subcellular localization and assembly of a novel mutation of KCNJ2 in Andersen's syndrome, *J. Mol. Cell. Cardiol. 35* (4), 409−415.

7. Chen, L., et al. (2002) A glutamate residue at the C terminus regulates activity of inward rectifier K^+ channels: implication for Andersen's syndrome, *Proc. Natl. Acad. Sci. U.S.A. 99* (12), 8430−8435.
8. Hille, B. (2001) *Ion Channels of Excitable Membranes*, 3rd ed., Sinauer Associates, Inc.,Sunderland, MA.
9. Nichols, C. G., and Lopatin, A. N. (1997) Inward rectifier potassium channels, *Annu. Rev. Physiol., 59*, 171−191.
10. Lu, Z., and MacKinnon, R. (1994) Electrostatic tuning of Mg^{2+} affinity in an inward-rectifier K^+ channel, *Nature 371* (6494), 243−246.
11. Lopatin, A. N., Makhina, E. N., and Nichols, C. G. (1994) Potassium channel block by cytoplasmic polyamines as the mechanism of intrinsic rectification, *Nature 372* (6504), 366−369.
12. Kubo, Y., and Murata, Y. (2001) Control of rectification and permeation by two distinct sites after the second transmembrane region in Kir2.1 K^+ channel, *J. Physiol. 531* (Pt 3), 645−660.
13. Fujiwara, Y., and Kubo, Y. (2006) Functional roles of charged amino acid residues on the wall of the cytoplasmic pore of Kir2.1, *J. Gen. Physiol. 127*, 401−419.
14. Pegan, S., et al. (2005) Cytoplasmic domain structures of Kir2.1 and Kir3.1 show sites for modulating gating and rectification, *Nat. Neurosci. 8* (3), 279−287.
15. Huang, C. L., Feng, S., and Hilgemann, D. W. (1998) Direct activation of inward rectifier potassium channels by PIP2 and its stabilization by Gbetagamma, *Nature 391* (6669), 803−806.
16. Kuo, A., et al. (2003) Crystal structure of the potassium channel KirBac1.1 in the closed state, *Science 300* (5627), 1922−1926.
17. Long, S. B., Campbell, E. B., and Mackinnon, R. (2005) Crystal structure of a mammalian voltage-dependent Shaker family K^+ channel, *Science 309* (5736), 897−903.
18. Lu, Z., Klem, A. M., and Ramu, Y. (2001) Ion conduction pore is conserved among potassium channels, *Nature 413* (6858), 809−813.
19. Silverman, S. K., Lester, H. A., and Dougherty, D. A. (1996) Subunit stoichiometry of a heteromultimeric G protein-coupled inward-rectifier K^+ channel, *J. Biol. Chem. 27148*, 30524−30528.
20. Fink, M., et al. (1996) Dominant negative chimeras provide evidence for homo and heteromultimeric assembly of inward rectifier K^+ channel proteins via their N-terminal end, *FEBS Lett. 378* (1), 64−68.
21. Bendahhou, S., et al. (2003) Defective potassium channel Kir2.1 trafficking underlies Andersen-Tawil syndrome, *J. Biol. Chem. 278* (51), 51779−51785.
22. Zaritsky, J. J., et al. (2001) The consequences of disrupting cardiac inwardly rectifying K^+ current (I(K1)) as revealed by the targeted deletion of the murine Kir2.1 and Kir2.2 genes, *J. Physiol. 533* (Pt 3), 697−710.
23. Kubo, Y., et al. (1993) Primary structure and functional expression of a mouse inward rectifier potassium channel, *Nature 362* (6416), 127−133.
24. Finley, M., et al. (2004) betaL-betaM loop in the C-terminal domain of G protein-activated inwardly rectifying K^+ channels is important for G(betagamma) subunit activation, *J. Physiol. 555* (Pt 3), 643−657.
25. Zhou, Y., et al. (2001) Chemistry of ion coordination and hydration revealed by a K^+ channel-Fab complex at 2.0 Å resolution, *Nature 414* (6859), 43−48.
26. Periole, X., et al. (1997) Simple two-body cation−water interaction potentials derived from ab initio calculations. Comparison to results obtained with an empirical approach, *J. Phys. Chem. 101*, 5018−5025.
27. Bendahhou, S., et al. (2005) In vivo and in vitro functional characterization of Andersen's syndrome mutations, *J. Physiol. 565* (Pt 3), 731−741.
28. Nishida, M., and MacKinnon, R. (2002) Structural basis of inward rectification: cytoplasmic pore of the G protein-gated inward rectifier GIRK1 at 1.8 Å resolution, *Cell 111* (7), 957−965.

BI060653D